ORIGINAL PAPER

Electrospun PEO nanofibrous membrane enable by LiCl, LiClO₄, and LiTFSI salts: a versatile solvent-free electrolyte for lithium-ion battery application

Seyedeh Nooshin Banitaba [1] · Dariush Semnani [1] · Aref Fakhrali [1] · Seyed Vahid Ebadi [1] · Elahe Heydari-Soureshjani [2] · Behzad Rezaei [2] · Ali A. Ensafi [2]

Abstract

In this study, the effect of type of lithium salts on the main properties of the nanostructure electrolytes was studied. Electrospinning process was applied to production of solvent-free PEO-based nanofibrous electrolytes containing various lithium salts, i.e., LiCl, LiClO₄, and LiTFSI. Then, the characteristics of the electrospun nanofibers were evaluated by various techniques. The fraction of free ions was estimated by the FTIR spectrum. Also, to investigate the crystalline phases of the as-spun electrolytes, the samples were subjected to X-ray analysis. The highest room temperature ionic conductivity of the fabricated electrolytes was obtained as 0.33 mS cm⁻¹ by the addition of 1.5 wt% LiClO₄ into the nanofibers. Furthermore, the cycling stability of the as-spun structures was enhanced by increasing the amount of LiClO₄ and LiCl salts in the produced nanofibers. The results implied that the prepared nanofibers are good candidates as solvent-free electrolytes for Li-ion batteries.

Keywords Nanofibrous electrolyte · Lithium salts · SPEs · Ionic conductivity · Li-ion battery

Introduction

Rechargeable energy storage devices are required for a wide variety of applications such as portable power tools and electrical vehicles. Lithium secondary battery (LIB) has been identified as a great candidate for the energy storage application due to high energy density and long cycle life [1, 2]. However, the usage of liquid electrolytes in LIBs has some major challenges such as dendrite formation and low safety [3, 4]. In recent years, extensive researches have been conducted on the replacement of liquid electrolytes with solid-state electrolytes. The solid polymer electrolytes (SPEs) are one of the most promising approaches toward fabrication of safe, light-weight, and flexible LIBs [5, 6]. Although, the poor ionic conductivity at room temperature (about 10^{-6} mS cm⁻¹) hindered their practical applications [7]. In general, SPEs are prepared by dispersion of an alkali salt in a polymer matric. Commonly, SPEs are synthesized in the form of polymeric thin films by using a standard film casting method [7, 8]. Ionic conductivity of the SPEs is influenced by the total amorphous regions and glass transition temperature (Tg) of the fabricated polymeric membranes. As crystalline phases and Tg decrease, ionic conductivity increases [7, 9]. Among all the polymeric matrices, polyethylene oxide (PEO) has been studied as the best polymer matric. PEO with a high dielectric constant (ε~5) is capable to dissolve various salts and additives. The low Tg of PEO (Tg = − 63 °C) leads to the high local motions of the polymer chains, which enhances the ionic conductivity. Moreover, PEO has shown high electrochemical stability against electrode materials [4, 10].

Lithium salt plays a significant role in various characteristics of the SPEs [11–13]. Lithium hexafluorophosphate (LiPF6), lithium perchlorate (LiClO4), lithium tetra fluoroborate (LiBF4), lithium chloride (LiCl), and lithium bis(trifluoromethanesulfonyl)imide (LiTFSI) are the most important lithium salts. The applied lithium salts in the SPE's

✉ Dariush Semnani
d_semnani@cc.iut.ac.ir

[1] Department of Textile Engineering, Isfahan University of Technology, Isfahan 84156-83111, Iran

[2] Department of Chemistry, Isfahan University of Technology, Isfahan 84156-83111, Iran

structures should be dissociated easily to provide the high mobility for the Li$^+$ ions [13, 14].

Numerous researches have been devoted to the study of the electrochemical properties of the lithium salts in nonaqueous solution electrolytes as well as the polymeric film electrolytes. Wang and Min [15] reported the high ionic conductivity of 2.25×10^{-7} S cm^{-1} for an SPE containing LiCl as a lithium salt. In addition, the ionic conductivity of $10^{-0.5}$ S cm^{-1} was reported for a thermoplastic starch electrolyte containing 18 wt% LiCl [16]. Baskaran et al. [17] showed an enhancement in the ionic conductivity of a PVAc:LiClO$_4$ SPE, from 7.6×10^{-7} S cm^{-1} to 6.2×10^{-5} S cm^{-1}, with increasing of LiClO$_4$ ratio from 10 to 20 wt%. Huh et al. [18] reported the highest ionic conductivity of 2.43×10^{-6} S cm^{-1} for poly(ethylene glycol)-polyurethane SPE containing LiClO$_4$ lithium salt at the oxygen-to-lithium cation mole ratio ([O]/[Li$^+$]) of 16. Ghelichi et al. [10] illustrated that the ionic conductivity of PEO/PMMA SPE has improved with increasing the amount of LiClO$_4$ salt up to the optimum ratio ([O]/[Li] = 50). However, the ionic conductivity of this SPE was reduced by further increment of the LiClO$_4$. Saleem Khan and Shakoor [19] also compared the effect of LiCl and LiClO$_4$ lithium salts on the ionic conductivity of the PEO-based solution-casted polymer electrolytes. Based on this study, the ionic conductivity could be improved from 1.38×10^{-8} S cm^{-1} to 3.16×10^{-7} S cm^{-1} and 6.13×10^{-7} S cm^{-1}, respectively. Watanabe and Nishimoto [20] showed that the ionic conductivity of an SPE could be enhanced from 10^{-4} S cm^{-1} to 3.5×10^{-3} S.cm^{-1} at 370 K with increasing the LiTFSI ratio from 0.02 to 0.08 wt%. In addition, Marzantowicz et al. [14] reported the highest ionic conductivity of 4×10^{-6} S cm^{-1} at room temperature for a PEO-LiTFSI SPE with the [O]/[Li$^+$] ratio of 8. Moreover, Stolwijk et al. [21] illustrated the improvement of the ionic conductivity from 0.5×10^{-5} S cm^{-1} to 0.8×10^{-3} S cm^{-1} with increasing the LiTFSI concentration in an SPE structure and reducing the [O]/[Li$^+$] ratio from 1000 to 60.

Newly, electrospinning has been identified as a versatile method for the fabrication of highly-porous membranes containing high surface-to-volume ratio nanofibers. Recent researches compared the polymeric films with the electrospun membranes and showed the superior ionic conductivity of the electrospun membranes. High porosity along with the small and tiny pores improves the ion motions in the nanofibrous polymeric electrolytes and so favors their electrochemical performance. In addition, presence of the unwanted salt-polymer crystalline regions ((LiX)$_x$ PEO) in the solution-casted membranes results in trapping of the Li$^+$ ions and so reduction of the ionic conductivity. The aforementioned crystalline phases are formed due to slow evaporation rate of the solvent from the solution-casted mats. However, these unwanted crystalline regions are absent in the nanofibrous membranes. High surface to volume ratio of the polymer jet accelerates the evaporation rate of the solvent in the electrospinning electrical field

and therefore, does not allow the polymer chains and the salt molecules to create such crystalline regions [22–24]. There is few research that used electrospun membrane as SPE. For example, Freitage et al. [24] reported the ionic conductivity of 0.2 mS.cm^{-1} at room temperature for a PEO-succinonitrile (SN)-LiBF$_4$ nanofibrous SPE. Walke et al. [25] investigated the effect of LiTFSI on the ionic conductivity of a nanofibrous PEO-SN electrolyte. The ionic conductivity of 2.8×10^{-4} S cm^{-1} was reported for the electrospun PEO-SN-LiTFSI electrolyte. However, the polymeric film electrolyte with similar chemical composition illustrated 5×10^{-5} S cm^{-1} ionic conductivity. In previous works, electrospun PEO-based electrolytes incorporated with inert ceramic fillers including zinc oxide and titanium dioxide were evaluated, which showed superior ionic conductivity than the solution cast ones [22, 26]. In this study, nanostructured electrolytes containing different lithium salts including LiCl, LiClO$_4$, and LiTFSI were prepared via electrospinning method for LIB applications. The effects of these lithium salts on the structural and electrochemical properties of produced nanofibrous PEO-based electrolytes were investigated.

Experimental

Materials

Polyethene oxide (PEO, MW = 300,000) and lithium chloride (LiCl) were purchased from Sigma-Aldrich (USA), and lithium perchlorate (LiClO$_4$) and lithium bis(trifluoromethanesulfonyl)imide (LiTFSI) were supplied by Alfa Aesar (Germany) and ACROSS organics (Germany), respectively. Also, acetonitrile and ethylene carbonate (EC) were obtained from Merck (Germany). All chemicals were used without any purification.

Preparation of the polymer solutions and the electrospun electrolytes

PEO polymer powder and EC plasticizer were added to acetonitrile with weight ratios of 7 and 9 wt%, respectively. Each of lithium salts, including LiClO$_4$ and LiTFSI with various concentrations of 0.5, 1, 1.5, and 2 wt%, was added to the prepared mixtures, separately. For the preparation of the PEO-based nanofibrous electrolytes containing LiCl as lithium salt, 7 wt% PEO, 9 wt% EC, and various ratios of LiCl salt including 0.5, 1, and 1.5 wt% were added to distilled water. The obtained mixtures were stirred vigorously for 24 h at ambient temperature to gain homogenous solutions. In order to compare the effect of the solvent on various characteristics of the nanofibrous samples, polymer solutions of PEO-EC-1 wt%, LiClO$_4$, and PEO-EC- 1 wt% LiTFSI were also prepared by using the distilled water as the solvent.

PEO-based nanofibrous electrolytes were fabricated by electrospinning of the as-prepared polymer solutions. The schematic representation of the applied horizontal electrospinning set-up is shown in Fig. 1. The polymer solution was loaded in a 1-ml plastic syringe with a stainless-steel needle (gauge 20). The polymer solution was fed with a rate of 0.5 ml h^{-1} by an infusion pump. A rotational drum was used to collect the electrospun nanofibers. The distance between the syringe needle and the collector was kept constant at 15 cm. A high-voltage power supplier was utilized to apply an 18.4 kV between the syringe needle and the collector. The attributed codes to the electrospun samples are listed in Table 1. The electrospun membranes were stored in a desiccator under vacuum for further characterization.

Characterization of the electrospun electrolytes

Surface morphology of the electrospun nanofibers was characterized by field emission scanning electron microscopy (FESEM, NOVA NANOSEM 230, Philips CM120). The average diameter of the nanofibers was examined through a hundred measurements by using ImageJ software (National Institutes of Health, Bethesda, MD). The Fourier-transform infrared spectrophotometer (FT-IR, BOMEM-MB100) in the wavenumber region between 4000 and 400 cm^{-1} was used to record the spectra of the electrospun nanofibers. The fraction of free lithium ions (%) was examined from the FTIR spectrum using Eq. (1):

$$\text{Fraction of free Li ions }(\%) = \frac{\text{The area under the anion peak}}{\text{The area under the ion pair peak}} \quad (1)$$

The X-ray diffraction (Philips X'pert MPD) in the diffraction angle range of $2\theta = 10\text{–}60^0$ was used to estimate the crystalline phases (%) of the electrospun electrolytes according to Eq. (2).

$$\text{Crystalline phases }(\%) = \frac{\text{Total area of the crystalline peaks}}{\text{Total area of all peaks}} \quad (2)$$

Electrochemical analysis of the nanofibrous electrolytes

Electrochemical impedance spectroscopy (EIS, Autolab: PGSTAT302N, EcoeChemie, The Netherlands) in the frequency range of 1 MHz to 0.01 Hz was used to measure the ionic conductivity of the as-spun nanofibers. An oscillation voltage of 500 mV (open circuit potential) was applied to the cell configuration of stainless-steel electrode| nanofibrous electrolyte| stainless-steel electrode. The bulk resistance (R_b) was obtained from the interception of the semicircle and the tilted spike appeared in the high frequency and low frequency of the impedance spectra, respectively. The ionic conductivity (σ) of the as-spun electrolytes was calculated by following Eq. (3).

$$\sigma \left(\text{S.cm}^{-1}\right) = {}^{t}/_{S \times R_b} \quad (3)$$
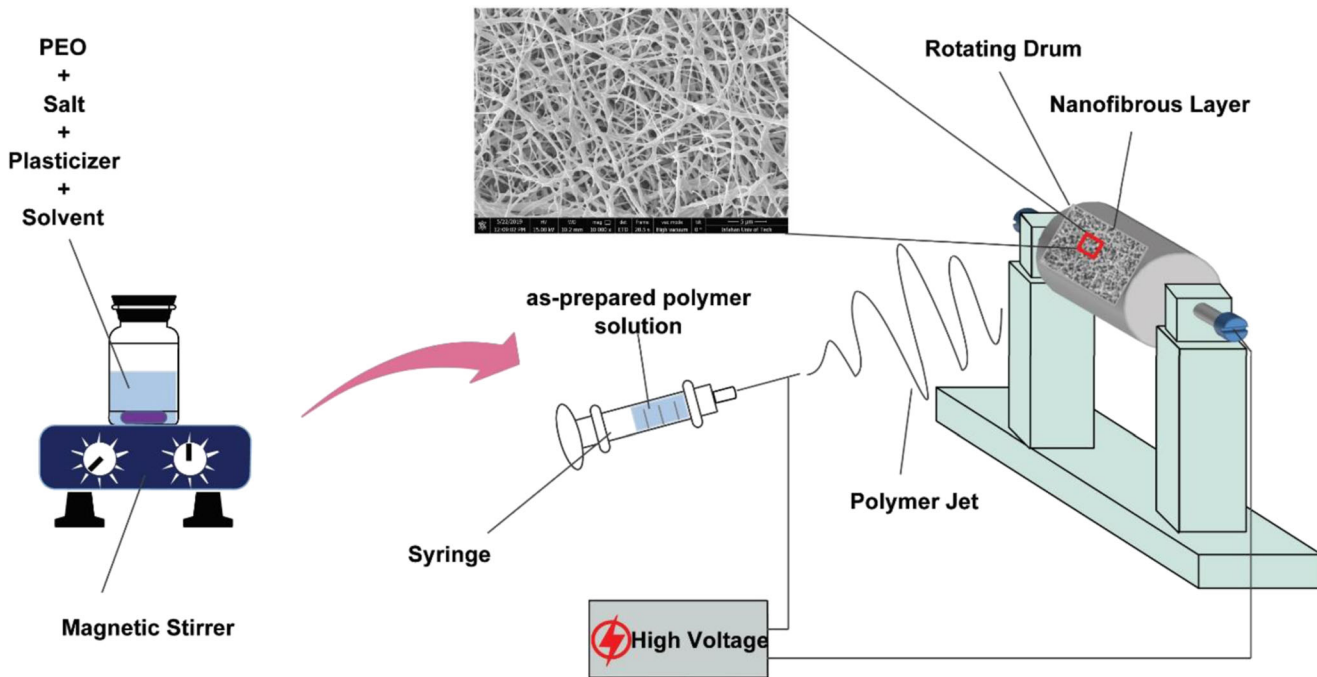

Fig. 1 Schematic illustration of electrospinning apparatus

Table 1 The average diameter, crystallinity, fraction of free ions, and Li-ion conductivity of the electrospun electrolytes

Sample ID	The electrospun polymer solution	Average fiber diameter (nm)	Crystalline regions (%)	Fraction of free Li ions (%)	Conductivity (mS.cm^{-1})
FFS	PEO-EC-acetonitrile	425 ± 216	15.61	-	-
LiCl@PEO 1	PEO-EC-0.5 wt% LiCl-acetonitrile	363 ± 132	14.85	59.2	0.061
LiCl@PEO 2	PEO-EC-1 wt% LiCl-acetonitrile	410 ± 175	16.04	63.8	0.084
LiClO$_4$@PEO 1	PEO-EC-0.5 wt% LiClO$_4$-acetonitrile	890 ± 371	16.48	64.2	0.009
LiClO$_4$@PEO 2	PEO-EC-1 wt% LiClO$_4$-acetonitrile	1133 ± 402	18.19	67.5	0.042
LiClO$_4$@PEO 3	PEO-EC-1.5 wt% LiClO$_4$-acetonitrile	1339 ± 754	19.27	71.8	0.33
LiTFSI@PEO 1	PEO-EC-0.5 wt% LiTFSI-acetonitrile	417 ± 199	14.24	72.5	0.062
LiTFSI@PEO 2	PEO-EC-1 wt% LiTFSI-acetonitrile	427 ± 241	15.55	77.8	0.073
LiTFSI@PEO 3	PEO-EC-1.5 wt% LiTFSI-acetonitrile	698 ± 382	17.32	58.5	0.034
LiClO$_4$@PEO-W	PEO-EC-1 wt% LiClO$_4$-distilled water	421 ± 177	19.43	50.3	0.033
LiTFSI@PEO-W	PEO-EC-1 wt% LiTFSI distilled water	610 ± 425	16.25	51.6	0.031

Where, t (cm) and S (cm^2) are the thickness and the area of the electrolyte, respectively. The activation energy (Ea) of the fabricated electrolytes was evaluated by providing the temperature dependence conductivity in the temperature range of 298 to 313 K and Eq. (4).

$$\sigma = \sigma_0 \exp\left(\frac{-Ea}{R \times T}\right) \quad (4)$$

Where, σ_0 is pre-exponential factor, T (K) is temperature, and R is universal gas constant (8.314 J.K^{-1}.mol^{-1}). The polarizing ability of the prepared SPEs was evaluated by calculating the dielectric permittivity (ε^*). The ε^* is a complex quantity presented in Eq. (5).

$$\varepsilon^* = \varepsilon_r - j\varepsilon_i \quad (5)$$

Where, ε_r and ε_i are dielectric constant and dielectric loss, respectively. The dielectric parameters can be obtained through Eqs. (6) and (7):

$$\varepsilon_r = \frac{Z_{Im}}{\omega C_0 \left(Z_{Re}^2 + Z_{Im}^2\right)} \quad (6)$$

$$\varepsilon_i = \frac{Z_{Re}}{\omega C_0 \left(Z_{Re}^2 + Z_{Im}^2\right)} \quad (7)$$

Here, $C_0 = \frac{\varepsilon_0 . S}{t}$ is the vacuum capacitance, ε_0 is permittivity of free space (8.854 × 10^{-12} F m^{-1}), S is the area and t is the thickness of the electrolyte. In addition, ω is equal to $2\pi f$, where f is the frequency of the applied ac field. The dissipation factor or the ratio of energy loss to energy stored was also obtained by using Eq. (8).

$$\tan(\delta) = \frac{\varepsilon_i}{\varepsilon_r} \quad (8)$$

The electrospun membranes were also sandwiched in a symmetric cell between two stainless-steel electrodes to examine the cycling durability by using a potentiostat/galvanostat (pocket STAT Model). Discharge capacity was measured by applying a constant current density between the voltages of − 1 to 1 V at room temperature.

Results and discussion

The FESEM images of the electrospun electrolytes are shown in Fig. 2. As can be seen, the homogenous and bead-free nanofibers were obtained in all samples. The average diameter of the nanofibers is listed in Table 1. According to the obtained results, thinner nanofibers were formed by adding of 0.5 wt% LiCl and LiTFSI into the polymer solutions. However, the average diameter of the nanofibers increased beyond this quantity. In addition, the average diameter of the nanofibers containing LiClO$_4$ lithium salt was increased by an increment of the LiClO$_4$ ratio. The variation on the nanofiber diameters by the addition of lithium salts can be attributed to the effects of the salts on the electrospinning procedure. First, the electron conductivity of the polymer solutions enhances with the introduction of the salt particles into the polymer solutions. Higher electron conductivity of the polymer solutions causes more repulsive columbic force between the solution particles which leads to the higher elongation rate of the polymer jet. When the elongation rate increases, the finer nanofibers are formed. Second, the expelled mass flow from the syringe needle increases by enhancement of the solution conductivity, which leads to the formation of thicker electrospun fibers. The average diameter of the electrospun nanofibers is impacted by one of the above-mentioned situations. The observed trends are in line with the previous studies. Choi et al. [27] observed formation of thinner nanofibers by the addition of benzyl trialkylammonium chlorides into a poly(3-hydroxybutyrate-co-3-hydroxyvalerate) polymer solution. While, Yalcinkaya et al. [28] reported an increment in the
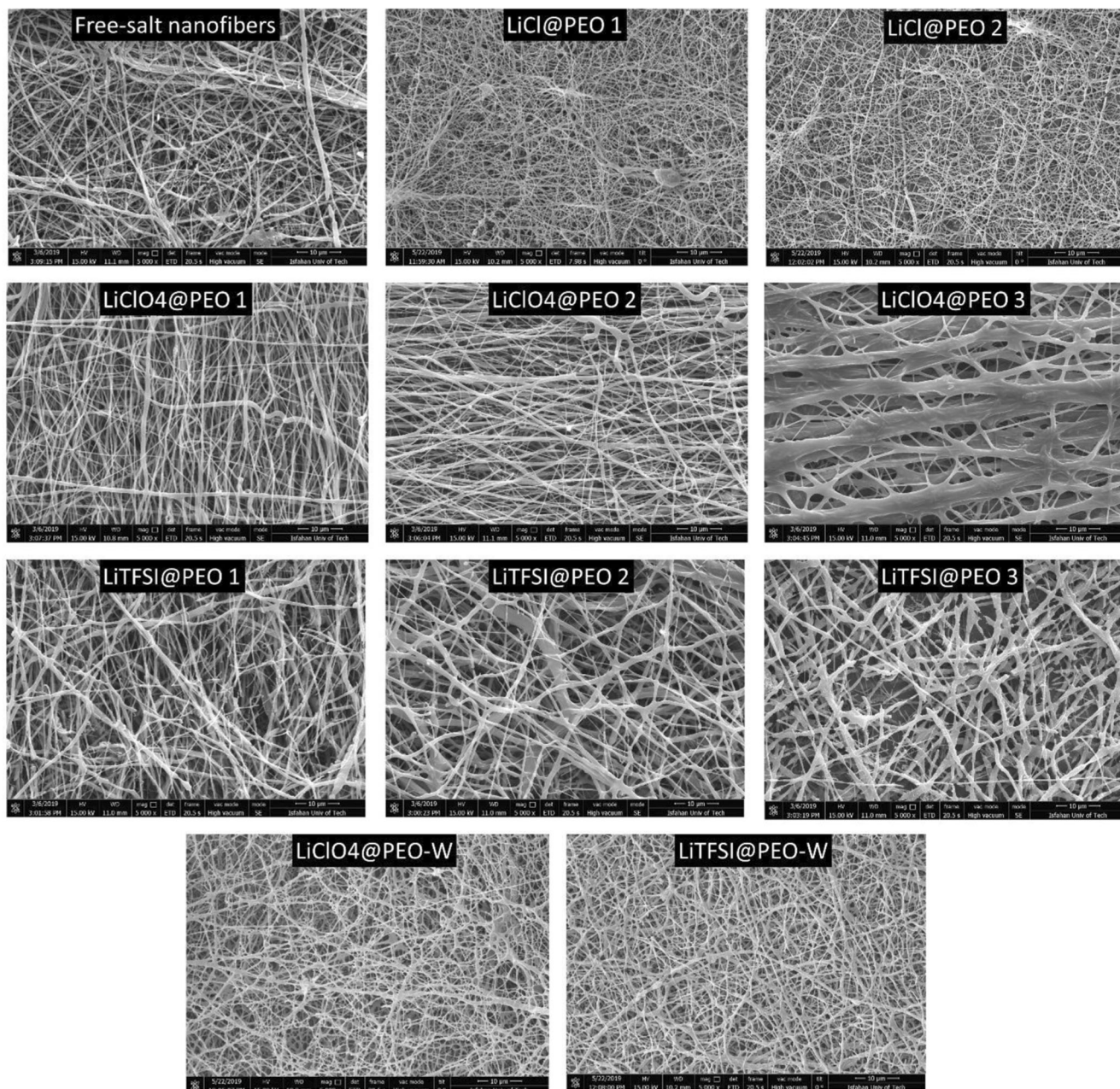
Fig. 2 FESEM images of the electrospun nanofibrous electrolytes

PEO-based nanofiber's diameter by the addition of LiCl lithium salt. Moreover, flat fibers were obtained in the as-spun nanofibers containing 1.5 wt% LiClO$_4$. This can be linked to lack of sufficient time for complete evaporation of the solvent due to the high rate of the ejected mass flow. Furthermore, when the water was used as solvent instead of acetonitrile, the reducing of the fiber diameter is further affected because of higher melting point of the water. It is worth to note that the electrospun nanofibers containing 1.5 and 2 wt% LiCl, 2 wt% LiClO$_4$, and 2 wt% LiTFSI could not be collected on the rotational drum. The reason may be attributed to the repulsion

of the fabricated nanofibers on the collector caused by the charge aggregation in the electrospun nanofibers.

Figure 3 shows the FT-IR spectra of the nanofibrous electrolytes. In free salt PEO-EC spectrum (I), the peaks at 2881 cm^{-1}, 1957 cm^{-1}, 1465 cm^{-1}, 1149 cm^{-1}, and 844 cm^{-1} are assigned to CH symmetric stretching, CH asymmetric stretching, CH$_2$ scissoring bending, C-O-C stretching, and CH$_2$ wagging bending, respectively. By the addition of LiClO$_4$ salt to the PEO-EC nanofibers, the band at 1957 cm^{-1} was shifted to 1959 cm^{-1} (II and III) and 1955 cm^{-1} (IV). In addition, incorporation of 1.5 wt% LiClO$_4$ into the as-spun
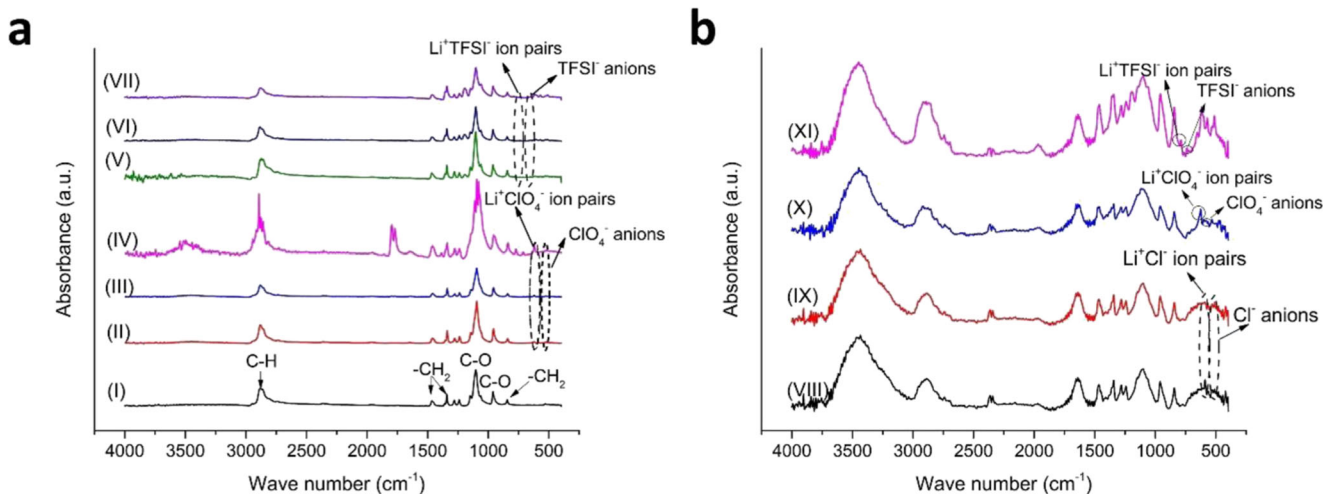
Fig. 3 FTIR spectra of the nanofibrous samples electrospun using (a) acetonitrile and (b) water solvents : (I) PEO-EC, (II) LiClO4@PEO 1, (III) LiClO4@PEO 2, (IV) LiClO4@PEO 3, (V) LiTFSI@PEO 1 and (VI) LiTFSI@PEO 2 , (VII) LiTFSI@PEO 3, (VIII) LiCl@PEO 1, (IX) LiCl@PEO 2, (X) LiClO4@PEO-W and (XI) LiTFSI@PEO-W

nanofibers shifted CH symmetric stretching and C-O-C stretching bands to 2893 cm^{-1} and 1141 cm^{-1}, respectively. The vibration of CH$_2$ wagging was also changed to 840 cm^{-1} (II and III) and 837 cm^{-1} (IV). In the LiTFSI-loaded electrospun nanofibers, the CH symmetric band was shifted to 2873 cm^{-1} (V) and 2885 cm^{-1} (VI and VII). In addition, C-O-C stretching was shifted to 1145 cm^{-1}. By incorporation of the LiCl salt into the electrospun membranes, the peaks at 2881 cm^{-1} and 1149 cm^{-1} were shifted to 2889 cm^{-1} and 1153 cm^{-1}, respectively. Changes in the wavenumber of the PEO characteristic peaks were also reported by several researchers [19, 29]. The observed changes in the wavenumber of the peaks confirm the complexation of the lithium salts with PEO-EC in the nanofibrous structures. In fact, the carbonyl group (C=O) in EC molecules is an electron donor which acts as a Lewis-base and enter in competition with the anions of the lithium salts and the ether groups of PEO polymer chains to interact with the Li$^+$ cations. So, the following interactions are formed in the prepared solutions: Li$^+$-anion (Cl$^-$, ClO$_4^-$ and TFSI$^-$) ion-ion interaction, Li$^+$-PEO ion-dipole interaction, and Li$^+$-EC ion-molecule interaction [30].

In the salt-loaded nanofibers, two peaks are appeared attributed to ion pairs (Li$^+$Cl$^-$, Li$^+$ClO$_4^-$, and Li$^+$TFSI$^-$) and free anions (Cl$^-$, ClO$_4^-$, and TFSI$^-$). In II, III, and IV spectra, the peaks at 621 cm^{-1} and 524 cm^{-1} are assigned to Li$^+$ClO$_4^-$ ion pairs and ClO$_4^-$ anions, respectively. By the addition of LiTFSI (V, VI, and VII), Li$^+$TFSI$^-$ ion pair peak, and TFSI$^-$, the peak appeared at 786 cm^{-1} and 736 cm^{-1}, respectively. Also, Li$^+$Cl$^-$ and Cl$^-$ peaks were observed at 590 cm^{-1} and 528 cm^{-1}, respectively, in VIII and IX spectra. According to the obtained spectra, the fraction of free ions was calculated and listed in Table 1. As can be seen, the fraction of free ions enhanced by increasing the LiCl and LiClO$_4$ ratios in the as-spun nanofibers. By an increment of the LiTFSI proportion up to 1 wt%, the fraction of free

ions increased. However, the fraction of free ions decreased beyond this amount. The observed reduction in the fraction of free ions can be linked with the agglomeration of the salt particles resulting from the larger size of TFSI$^-$ anions compared with ClO$_4^-$ and Cl$^-$ anions. Moreover, the order of free ions is as follows: LiCl@PEO < LiClO$_4$@PEO < LiTFSI@PEO. The reason can be attributed to the difference between the lattice energy of the applied lithium salts. The LiTFSI ion pairs are easily dissociated due to the lower lattice energy compared with two other lithium salts [29]. Furthermore, lower free ions were formed by applying the distilled water as the solvent (LiClO$_4$@PEO-W and LiTFSI@PEO-W). The reason may correspond to the higher melting point of the water in comparison with the acetonitrile. Therefore, it seems that evaporation of the distilled water takes more time, which provides the possibility for the agglomeration of the salt particles.

XRD spectra of the as-spun electrolytes are depicted in Fig. 4. The crystalline regions were obtained for all samples (see Table 1). The results showed that by introduction of LiCl and LiTFSI salts into the as-spun fibers, the crystalline phases were first decreased and then increased. In addition, the amorphous regions decreased by incorporation of LiClO$_4$ salt into the nanofibrous electrolytes. The observed trends can be assigned to the effects of salts on the morphology of the polymeric structures and the electrospinning procedure [31]. First, the addition of salts into the polymeric structures causes a reduction in the orientation of the polymer chains and as a result increases amorphous phases [29]. Second, the existence of the salt in polymeric solutions increases the solution conductivity, which leads to more stretching and so higher orientation of the polymer chains [27]. In addition, the nanofibrous samples loaded with LiTFSI presented lower crystalline regions compared with the electrolytes containing LiCl and LiClO$_4$. The reason could be due to the larger size of the
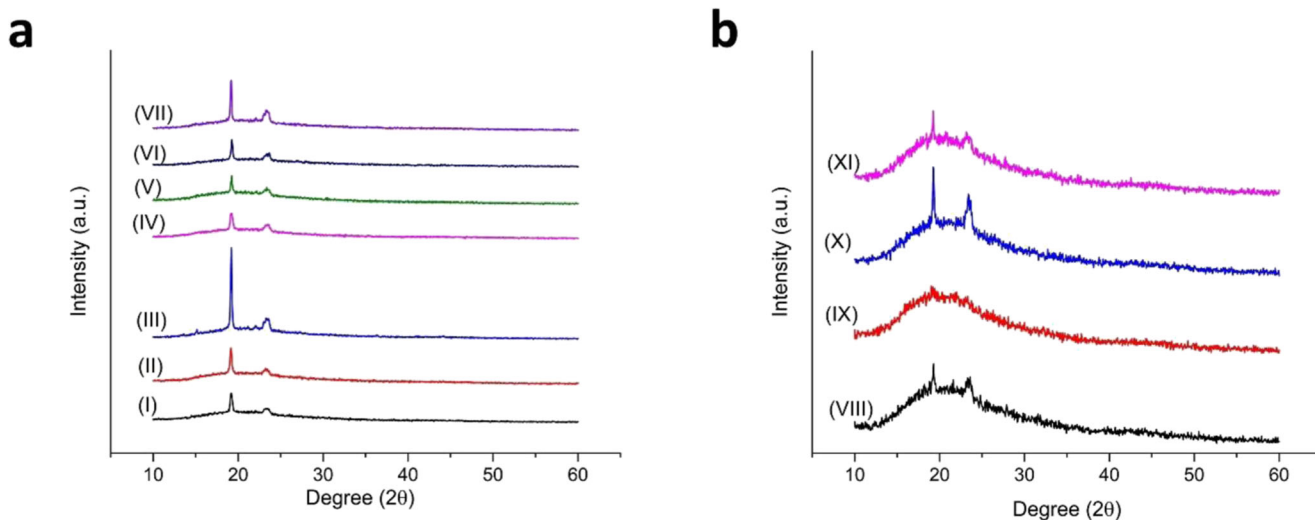
a

b

Fig. 4 XRD patterns of the electrospun samples fabricated using (a) acetonitrile and (b) water solvents :(I) PEO-EC, (II) LiClO4@PEO 1, (III) LiClO4@PEO 2, (IV) LiClO4@PEO 3, (V) LiTFSI@PEO 1, (VI) LiTFSI@PEO 2, (VII) LiTFSI@PEO 3, (VIII) LiCl@PEO 1, (IX) LiCl@PEO 2, (X) LiClO4@PEO-W and (XI) LiTFSI@PEO-W

$TFSI^-$ anions in comparison with the Cl^- and ClO_4^- anions. Moreover, using the distilled water instead of the acetonitrile led to the formation of more crystalline phases. This can be attributed to the slower evaporation rate of the distilled water, more bending instabilities in the electrospinning field and so formation of thinner fibers. As fiber diameter decreases, polymer chains are forced to place with more orientations which as a result enhances the crystalline regions.

As it has been reported in many researches, the crystalline peaks attributed to the PEO-salt crystalline phases are appeared in the degree ranges of $2\theta = 25$–$30°$ in the polymeric film electrolyte's spectra. The created crystalline regions trap lithium ions and so reduce the ionic conductivity [22, 24]. As can be apparently seen in the obtained XRD spectra (Fig. 4), these unwanted crystalline phases were absent in the as-spun structures. The reason may be assigned to the high surface to volume ratio of the electrospun jet which leads to the fast evaporation of the solvent in the electrospinning procedure. However, the slower rate of the solvent evaporation in the solution-casted polymer membranes allows the PEO polymer chains and the salt particles to form such crystalline phases [24].

In the SPEs, Li^+ ions migrate through the segmental motion of the polymer chains or via a hopping mechanism. A schematic representation (Fig. 5a) illustrates the free motion of Li^+ ions in a single nanofiber. Enhancement of the ionic conductivity by the addition of EC plasticizer was confirmed in the previous study [26]. Nyquist spectra of the electrospun electrolytes containing various lithium salts are presented in Fig. 5b–e. According to the obtained data, the ionic conductivity of the nanofibrous electrolytes enhanced with increasing of the LiCl and LiClO4 ratios. In accordance with the estimated fraction of free ions from FTIR spectra, the observed enhancement in the ionic conductivities can be linked with the rising of the

free Li^+ ions in the as-spun membranes. In addition, the bulk resistance decreased by increasing the LiTFSI concentration up to 1 wt%. However, the ionic conductivity reduced by incorporation of 1.5 wt% LiTFSI into the as-spun fibers due to the aggregation of the salt particles. Similar results have been examined by ShanShan Wang [29] and Zhao et al. [32]. The highest ionic conductivity of 0.33 mS cm^{-1} was obtained by loading 1.5 wt% LiClO4 into the as-spun structure. Moreover, the order of the ionic conductivity by the addition of 1 wt% lithium salts is LiClO4@PEO 2 < LiTFSI@PEO 2 < LiCl@PEO 2. As confirmed by FTIR and XRD spectra, a higher fraction of free Li^+ ions in the LiTFSI@PEO 2 nanofibrous electrolyte along with the lower crystalline phases compared with LiClO4@PEO 2 SPE caused the higher ionic conductivity. However, LiCl@PEO 2 sample showed the highest ionic conductivity despite the lowest fraction of free ions. This could be due to the existence of the finer fibers and so smaller pores in the mentioned electrospun membrane. Finer fibers provide more fiber-fiber contact points, which facilitate Li-ion migration between the nanofibers. In addition, transportation of the Li-ions through tiny pores of the as-spun membrane leads to the improvement of the ionic conduction [33]. Furthermore, applying the distilled water instead of acetonitrile as the solvent led to the reduction of the ionic conductivity may be due to the formation of more crystalline phases and lower free Li-ions (based on the obtained results from XRD and FTIR spectra).

The dependence of the ion conductivity versus temperature for the as-spun electrolytes containing various lithium salts is shown in Fig. 6. As can be seen, the ionic conductivity of the nanofibrous membranes was improved with increasing the temperature. Expansion of the polymer matrix with rising the temperature leads to increasing of the free volume. So,
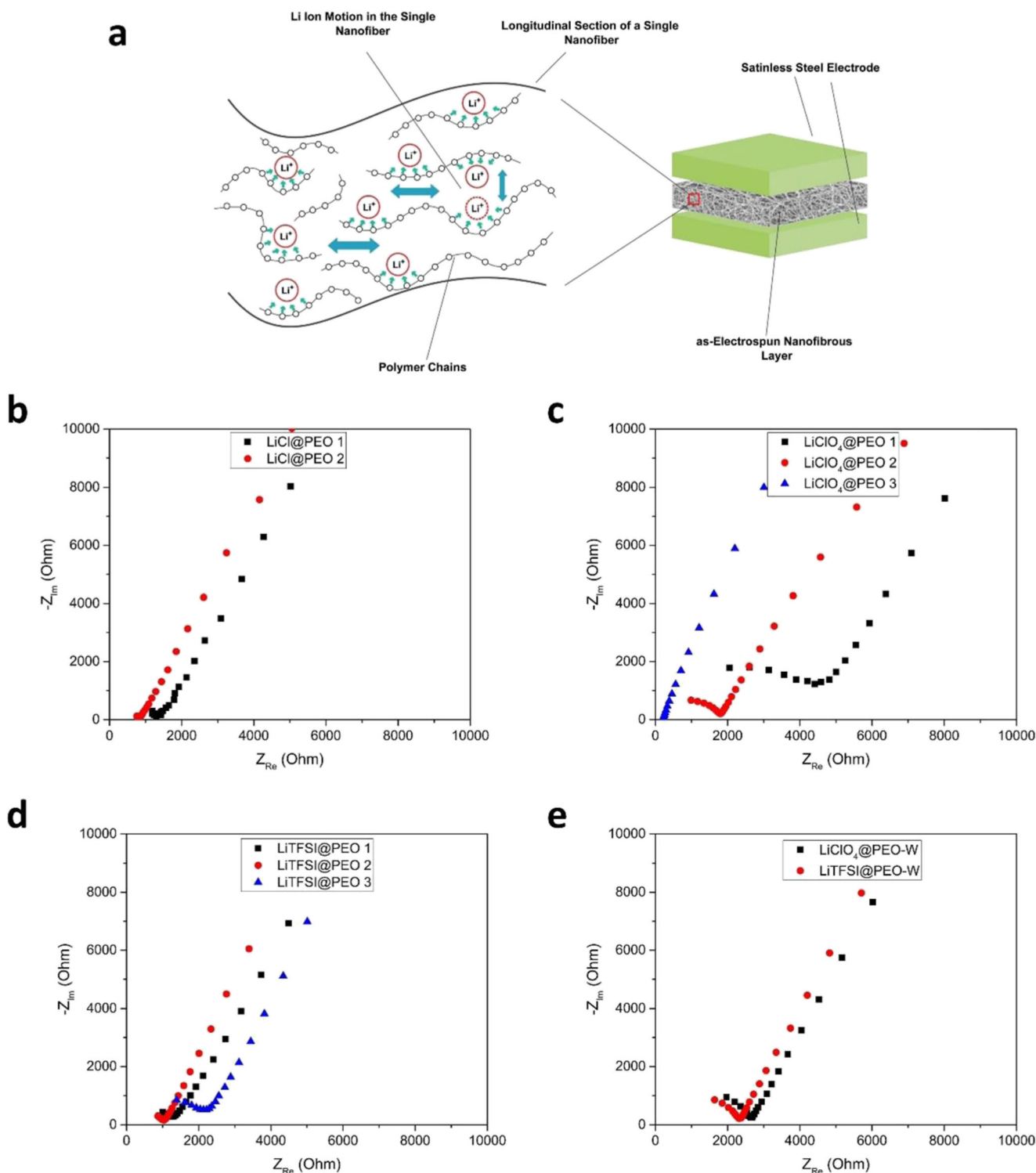
Fig. 5 **a** Schematic illustration of the Li$^+$ transport in single nanofiber. **b–e** Impedance spectra of the electrospun nanofibers containing various lithium salts

the ion conductivity is improved may be due to more movements of the polymer chains and higher motion of the Li$^+$ ions. In addition, according to the obtained regression lines (see Fig. 6), ion transportation in the as-spun electrolytes followed the Arrhenius behavior. So, the ionic conductivity in the

electrospun samples was mostly based on the hopping mechanism. The activation energy (Ea) was also calculated for the nanofibrous electrolytes (Fig. 6b). The results presented that the nanofibrous electrolytes containing LiClO$_4$ as salt exhibited lower Ea than the ones loaded with LiCl salt. Moreover,

the samples incorporated with 0.5 and 1 wt% LiTFSI presented the lowest Ea compared with two other lithium salts. The reason can be attributed to the difference between the sizes of Cl^-, ClO_4^-, and $TFSI^-$ anions. Small anions of Cl^- cause formation of a lattice network with high lattice energy. So, dissociation of the Li^+Cl^- ion pairs is more difficult than another lithium salts, which leads to a higher Ea. Although $TFSI^-$ is a large anion with a wide distribution of the negative charge around various atoms. Therefore, the bonding strength of the LiTFSI ionic salt is lower than two other lithium salts. Hence, the essential energy for the motion of Li^+ ions in the LiTFSI-loaded samples is the lowest [29].

Figure 7 displays the dielectric constant (ε_r) and dielectric loss (ε_i) factors as a function of frequency for the as-spun electrolytes. ε_r is a measure of energy stored in the SPE on application of an external electric field while ε_i shows the loss energy corresponding to the motion and alignment of ions and dipoles during the periodic reversal of the external electric field. Both ε_r and ε_i presented high values at low frequencies. However, the dielectric parameters reduced by increasing of the frequency. The reason can be linked with the reversal speed of the applied electric field. In low frequencies, the electric field reverses slowly. So, there is sufficient time for the alignment of the ions and dipoles which led to the higher ε_r and ε_i. However, the fast reversal speed of the polarity of the electric field at high frequencies does not allow the ions and dipoles to be aligned. Then, the dielectric parameters decrease with increasing of the frequency. Moreover, the electrospun electrolyte, loaded with 1.5 wt% $LiClO_4$ lithium salt, showed the highest values of ε_r and ε_i. The obtained results confirmed higher ionic conductivity of $LiClO_4$@PEO 3 sample compared with the other as-spun electrolytes.

The frequency dependence of the dissipation factor (loss tangent) of the electrospun electrolytes is presented in Fig. 8. It is apparent that the dissipation factor first increased and then decreased with increment of the frequency. The observable peaks in the plots are assigned to the electrode polarization frequency. The relaxation time (τ) can be obtained by the relaxation peak frequency (f) through the following equation ($\tau = \frac{1}{2\pi f}$). It can be seen that the relaxation time is inverse of the frequency. As relaxation time enhances, the ionic conductivity decreases [34]. According to the obtained data, the samples $LiClO_4$@PEO 1 and $LiClO_4$@PEO 3 showed, respectively, the highest and the lowest relaxation times. The results tied well with the calculated ionic conductivities of the samples through the Nyquist plots. Where, the $LiClO_4$@PEO 1 and $LiClO_4$@PEO 3 electrolytes presented the lowest and the highest ionic conductivities, respectively.

Solid-state polymer electrolytes provide fabrication of flexible and lightweight Li-ion batteries with high safety. However, performance deterioration against cycling has been widely reported for various polymer electrolytes. The cycling stability is mainly influenced by the mobility of the Li^+ ions and electrolyte-electrode interface. Formation of solid electrolyte interface (SEI) layer at the negative electrode is one of the probable reasons of the capacity fading. The SEI layer is created due the interaction between the electrode and residue existence of the solvents in the electrolyte membrane. In addition, low penetration rate of the Li^+ ions in the polymer matrix resulting from poor ionic conductivity could lead to the low cycling durability [35, 36]. Cycling stability of the nanofibrous electrolytes is shown in Fig. 9. As it can be clearly observed, the capacity retention was enhanced by increasing the loaded lithium perchlorate and lithium chloride ratios in
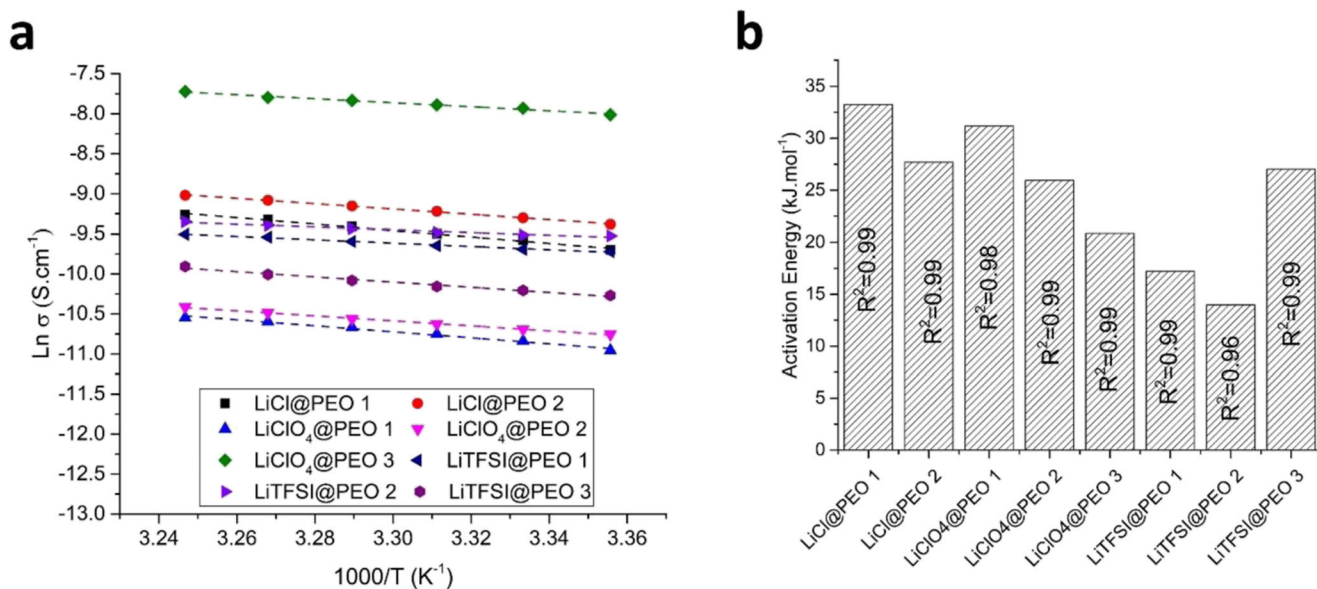

Fig. 6 a Conductivity versus temperature and b activation energy of the electrospun electrolytes
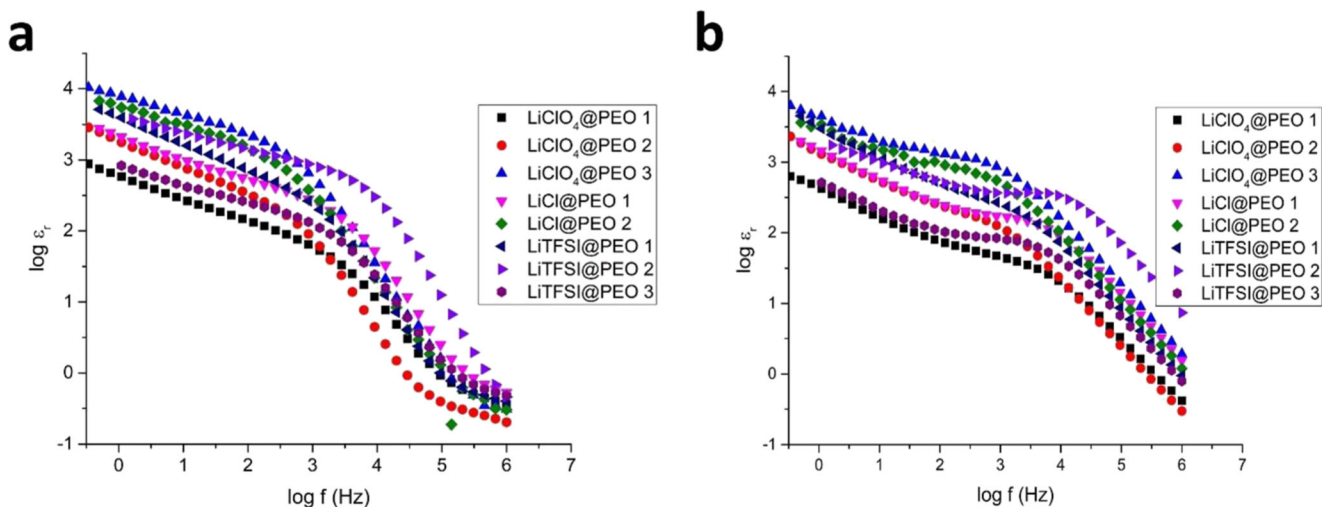
Fig. 7 Variation of **a** dielectric constant and **b** dielectric loss versus frequency for the as-spun electrolytes

the as-spun fibers. Based on the obtained data from FTIR and EIS spectra, it may be resulted from increment of the free Li$^+$ ions in the as-spun fibers and improvement of the ionic conductivity. In addition, the LiTFSI@PEO2 nanofibers (~90%) displayed higher capacity over cycling than the LiClO$_4$@PEO2 (~86%) electrolyte mat. Moreover, the as-spun sample incorporated with 1 wt% LiCl (~72%) showed the lowest capacity after 45 cycles in comparison with the ones embedded with 1 wt% LiTFSI and LiClO$_4$. Therefore, the observed trend may be referred to the differences between the fractions of free lithium ions in the electrospun membranes. Very recently, we presented the electrochemical properties of the filler-filled electrospun PEO-based electrolytes containing 1 wt% LiClO$_4$ and 4.5 wt% EC. Although inert ceramic fillers favor free Li$^+$ ions and facilitate Li$^+$ ion mobility, the nanofibrous samples incorporated with the TiO$_2$, SiO$_2$,

and Al$_2$O$_3$ nanoparticles revealed lower capacity retentions in the range of 32 to 65 % [37]. However, the insertion of MWCNT and GO nanofillers enhanced the cycling performance up to 85% resulting from the existence of the conductive fillers in the electrospun membranes [38]. So, the comparison between the obtained data confirms the role of the salt concentration on the cycling stability of the electrospun membranes.

Conclusion

In summary, nanofibrous polymer electrolytes comprising PEO, EC with LiCl, LiClO$_4$ and LiTFSI salts in various ratios were fabricated through the electrospinning process. The effects of the various lithium salts on the structural
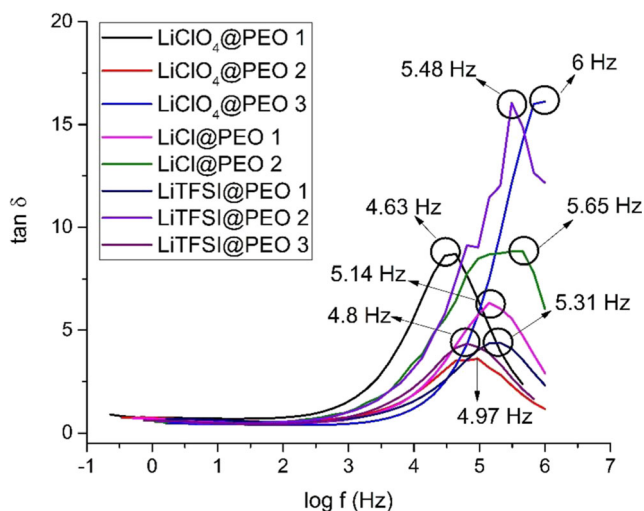

Fig. 8 Variation of dissipation factor with frequency for the nanofibrous electrolytes
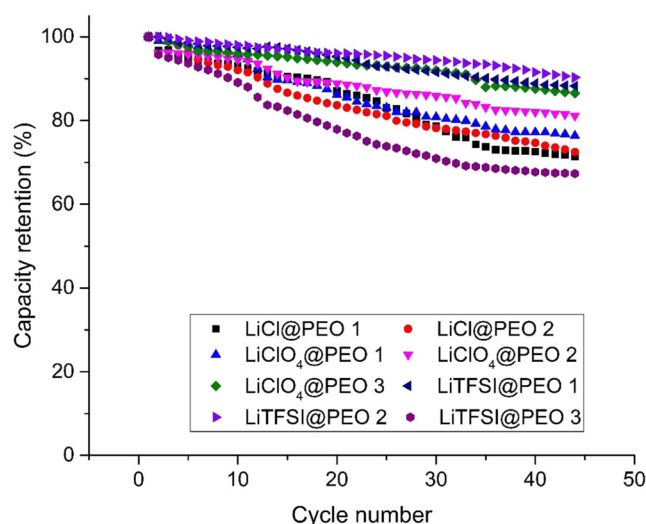

Fig. 9 Cycle stability of the as-spun membranes

characteristics (e.g., fiber diameters, a fraction of free Li$^+$ ions and crystalline regions) of the nanofibrous membranes were evaluated by using the FE-SEM, FTIR, and XRD analysis. The electrochemical measurement showed an enhancement in the ionic conductivity of the nanofibers by the addition of the lithium salts. It was found that the nanofibrous electrolyte containing 1.5 wt% LiClO$_4$ displayed the highest ionic conductivity of 0.33 mS cm^{-1} at room temperature. In addition, the ion migration obeyed Arrhenius relation in the as-spun electrolytes. The lowest activation energy of 13 kJ mol^{-1} was presented by the electrospun sample loaded with 1 wt% LiTFSI salt. Moreover, the as-spun structures retained more capacity by increasing the LiClO$_4$ and LiCl ratios. Overall, the results showed that solvent-free PEO-based nanofibers can be applied as new polymer structures and solvent-free electrolytes in lithium-ion battery application.

References

1. Lu L, Han X, Li J, Hua J, Ouyang M (2013) A review on the key issues for lithium-ion battery management in electric vehicles. J Power Sources 226:272–288
2. Nitta N, Wu F, Lee JT, Yushin G (2015) Li-ion battery materials: present and future. Mater Today 18:252–264
3. Etacheri V, Marom R, Elazari R, Salitra G, Aurbach D (2011) Challenges in the development of advanced Li-ion batteries: a review. Energy Environ Sci 4:3243–3262
4. Tarascon J-M, Armand M (2011) Issues and challenges facing rechargeable lithium batteries. In: Materials for sustainable energy: a collection of peer-reviewed research and review articles from Nature Publishing Group, World Scientific, pp. 171–179
5. Abraham K, Jiang Z (1996) A polymer electrolyte-based rechargeable lithium/oxygen battery. J Electrochem Soc 143:1–5
6. Verma P, Maire P, Novák P (2010) A review of the features and analyses of the solid electrolyte interphase in Li-ion batteries. Electrochim Acta 55:6332–6341
7. Croce F, Appetecchi GB, Persi L, Scrosati B (1998) Nanocomposite polymer electrolytes for lithium batteries. Nature 394:456–458
8. Murata K, Izuchi S, Yoshihisa Y (2000) An overview of the research and development of solid polymer electrolyte batteries. Electrochim Acta 45:1501–1508
9. Gadjourova Z, Andreev YG, Tunstall DP, Bruce PG (2001) Ionic conductivity in crystalline polymer electrolytes. Nature 412:520
10. Ghelichi M, Qazvini NT, Jafari SH, Khonakdar HA, Farajollahi Y, Scheffler C (2013) Conformational, thermal, and ionic conductivity behavior of PEO in PEO/PMMA miscible blend: investigating the effect of lithium salt. J Appl Polym Sci 129:1868–1874
11. Feng S, Shi D, Liu F, Zheng L, Nie J, Feng W, Huang X, Armand M, Zhou Z (2013) Single lithium-ion conducting polymer electrolytes based on poly [(4-styrenesulfonyl)(trifluoromethanesulfonyl) imide] anions. Electrochim Acta 93:254–263
12. Fullerton-Shirey SK, Maranas JK (2009) Effect of LiClO4 on the structure and mobility of PEO-based solid polymer electrolytes. Macromolecules 42:2142–2156
13. Yang R, Zhang SC, Zhang L, Bi XF (2013) In: Materials Science Forum, Trans Tech Publ, pp. 53–58
14. Marzantowicz M, Krok F, Dygas J, Florjańczyk Z, Zygadło-Monikowska E (2008) The influence of phase segregation on properties of semicrystalline PEO: LiTFSI electrolytes. Solid State Ionics 179:1670–1678
15. Wang S, Min K (2010) Solid polymer electrolytes of blends of polyurethane and polyether modified polysiloxane and their ionic conductivity. Polymer 51:2621–2628
16. Ning W, Xingxiang Z, Haihui L, Jianping W (2009) N, N-dimethylacetamide/lithium chloride plasticized starch as solid bio-polymer electrolytes. Carbohydr Polym 77:607–611
17. Baskaran R, Selvasekarapandian S, Kuwata N, Kawamura J, Hattori T (2007) Structure, thermal and transport properties of PVAc–LiClO4 solid polymer electrolytes. J Phys Chem Solids 68:407–412
18. Huh P-H, Choi M-G, Jo NJ, Lee J-K, Lee J-O, Yang W (2004) Effect of salt concentration on the glass transition temperature and ionic conductivity of poly(ethylene glycol)-polyurethane/LiClO4 complexes. Macromol Res 12:422–426
19. Khan MS, Shakoor A (2015) Ionic conductance, thermal and morphological behavior of PEO-graphene oxide-salts composites, J Chem, 2015
20. Watanabe M, Nishimoto A (1995) Effects of network structures and incorporated salt species on electrochemical properties of polyether-based polymer electrolytes. Solid State Ionics 79:306–312
21. Stolwijk NA, Wiencierz M, Heddier C, Kösters J (2012) What can we learn from ionic conductivity measurements in polymer electrolytes? A case study on poly (ethylene oxide)(PEO)–NaI and PEO–LiTFSI. J Phys Chem B 116:3065–3074
22. Banitaba SN, Semnani D, Heydari-Soureshjani E, Rezaei B, Ensafi AA (2019) Effect of titanium dioxide and zinc oxide fillers on morphology, electrochemical and mechanical properties of the PEO-based nanofibers, applicable as an electrolyte for lithium-ion batteries, Materials Research Express
23. Banitaba SN, Semnani D, Rezaei B, Ensafi AA (2019) Morphology and electrochemical and mechanical properties of polyethylene-oxide-based nanofibrous electrolytes applicable in lithium ion batteries. Polym Int 68:746–754
24. Freitag KM, Kirchhain H, Wüllen LV, Nilges T (2017)) Enhancement of Li ion conductivity by electrospun polymer fibers and direct fabrication of solvent-free separator membranes for Li ion batteries. Inorg Chem 56:2100–2107
25. Walke P, Freitag KM, Kirchhain H, Kaiser M, van Wüllen L, Nilges T (2018) Electrospun Li (TFSI)@ polyethylene oxide membranes as solid electrolytes. Z Anorg Allg Chem 644:1863–1874
26. Banitaba SN, Semnani D, Rezaei B, Ensafi AA (2019) Evaluating the electrochemical properties of PEO-based nanofibrous electrolytes incorporated with TiO2 nanofiller applicable in lithium-ion batteries. Polym Adv Technol
27. Haider A, Haider S, Kang I-K (2018) A comprehensive review summarizing the effect of electrospinning parameters and potential applications of nanofibers in biomedical and biotechnology. Arab J Chem 11:1165–1188
28. Yalcinkaya F, Yalcinkaya B, Jirsak O (2015) Influence of salts on electrospinning of aqueous and nonaqueous polymer solutions. J Nanomater 2015:1
29. S. Wang (2007) in, University of Akron
30. Qian X, Gu N, Cheng Z, Yang X, Wang E, Dong S (2002) Plasticizer effect on the ionic conductivity of PEO-based polymer electrolyte. Mater Chem Phys 74:98–103
31. Heikkilä P, Harlin A (2009) Electrospinning of polyacrylonitrile (PAN) solution: effect of conductive additive and filler on the process. Express Polym Lett 3:437–445
32. Zhao Y, Tao R, Fujinami T (2006) Enhancement of ionic conductivity of PEO-LiTFSI electrolyte upon incorporation of plasticizing lithium borate. Electrochim Acta 51:6451–6455

33. Vorrey S, Teeters D (2003) Study of the ion conduction of polymer electrolytes confined in micro and nanopores. Electrochim Acta 48: 2137–2141

34. Arya A, Sharma A (2018) Structural, microstructural and electrochemical properties of dispersed-type polymer nanocomposite films. J Phys D Appl Phys 51:045504

35. Song M-K, Cho J-Y, Cho BW, Rhee H-W (2002) Characterization of UV-cured gel polymer electrolytes for rechargeable lithium batteries. J Power Sources 110:209–215

36. Liu W (2016) Multilayer composite solid electrolytes for lithium ion batteries

37. Banitaba SN, Semnani D, Heydari-Soureshjani E, Rezaei B, Ensafi AA (2019) Electrospun polyethylene oxide-based membranes incorporated with silicon dioxide, aluminum oxide and clay nanoparticles as flexible solvent-free electrolytes for lithium-ion batteries. JOM 71:4537–4546

38. Banitaba SN, Semnani D, Heydari-Soureshjani E, Rezaei B, Ensafi AA (2019) Nanofibrous poly (ethylene oxide)-based structures incorporated with multi-walled carbon nanotube and graphene oxide as all-solid-state electrolytes for lithium ion batteries. Polym Int 68: 1787–1794